Electronic Supplementary Material (ESI) for ChemComm.

Electronic Supplementary Information for

A singlet ground state for a cobalt(II)-anilinylsalen radical complex

Amélie Kochem, Gisèle Gellon, Olivier Jarjayes, Christian Philouze, Nicolas Leconte, Maurice van Gastel, Eckhard Bill and Fabrice Thomas

Computational details. All electronic structure calculations presented were carried out using the ORCA program package. [1] Full geometry optimizations were performed for all complexes using the GGA functional BP86 [2,3] in combination with the Def2-TZV/P [4] basis set for all atoms and by taking advantage of the resolution of the identity (RI) approximation in the Split-RI-J variant [5] with the appropriate Coulomb fitting sets. [6] Increased integration grids (Grid4 in ORCA convention) and tight SCF convergence criteria were used. Solvent effects were accounted for according to the experimental conditions. For that purpose, we used the CH_2Cl_2 ($\mathcal{E}$ = 38.3) solvent within the framework of the conductor like screening (COSMO) dielectric continuum approach. [7] The relative energies were obtained from single-point calculations using the B3LYP functional [2,3] together with the Def2-TZV/P67 basis set. They were computed from the gas-phase optimized structures as a sum of electronic energy, thermal corrections to free energy, and free energy of solvation. Optical properties were also obtained from single-point calculations using the hybrid functional B3LYP [8,9] and the Def2-TZV/P67 basis set. Electronic transition energies and dipole moments for all models were calculated using time-dependent DFT (TD-DFT) [10-12] within the Tamm-Dancoff approximation. [13,14] To increase computational efficiency, the RI approximation [15] was used in calculating the Coulomb term and at least 30 excited states were calculated in the TDDFT calculations.

Materials and methods: All chemicals were of reagent grade and were used without purification. CH_2Cl_2 is anhydrous (> 99.8 %) and stored under Ar atmosphere. NMR-spectra were recorded at room temperature using a Bruker DRX 400 spectrometer operating at 400.13 MHz for 1H. Chemical shifts are given relative to tetramethylsilane (TMS) (listed in ppm). Mass spectra were recorded on a Thermofinningen (EI/DCI) or a Nermag R101C (FAB+) apparatus. Microanalysis were performed at the Mikroanalytisches Laboratorium KOLBE (Mülheim an der Ruhr). 298 K UV-Vis-NIR spectra were recorded on a Perkin Elmer Lambda 1050 spectrophotometer (the contribution of CH_2Cl_2 was removed by recording a baseline before measurements). Magnetic susceptibility data were measured from powder samples as well as frozen in the temperature range 2 - 300 K, and 2 – 140 K, respectively by using a SQUID susceptometer with a field of 1.0 T (MPMS-7, Quantum Design, calibrated with standard palladium reference sample, error <2%). The frozen solution sample was measured in a 4mm quartz tube with a compensation tube attached to the bottom, and the contribution from the solvent was subtracted by using a reference measurement with solvent only. To this end corresponding SQUID response functions for every field and temperature have been evaluated and subtracted separately with an own routine. The experimental data were corrected for underlying diamagnetism by use of tabulated Pascal's constants, as well as for temperature-independent paramagnetism. The susceptibility and magnetization data were simulated with our own package julX for exchange coupled systems (by E.B.) which does not use an approximate equation but full matrix diagnalization. The simulations were based on the usual spin-Hamilton operator for magnetically coupled dinuclear complexes with two spins $S_i = 1/2$:

$$H = g\mu_B(S_1+S_2)\cdot B - 2J\, S_1\cdot S_2 \qquad \text{eq. 1}$$

where g is the average electronic g value, J is the exchange coupling constant, and B is the induction strength of the applied magnetic field. After diagonalization of the Hamiltonian matrix, magnetic moments were calculated from the obtained eigenfunctions by using the Hellmann−Feynman theorem: $\mu_i(B) = \langle\psi_i|\partial\hat{H}/\partial B|\psi_i\rangle$. Molar magnetizations then were taken from thermal average of the components of μ_i along *B* for all magnetic levels, and the magnetization values as function of temperature and field were converted into molar susceptibility values by division by the induction *B*. Paramagnetic impurities were added to the simulation by using the vanVleck equation, and intermolecular interactions were considered by using a Weiss temperature, Θ_W, as perturbation of the temperature scale, kT' = k(T-Θ_W) for the calculation.

$(2)^{+}$•SbF_6^{-}: To a solution of **2** (0.1 g, 0.166 mmol) in CH_2Cl_2 (5 mL) was added 1.1 eq of $AgSbF_6$ (0.063 g, 0.183 mmol) under an inert atmosphere. This solution was stirred for 20 minutes at room temperature until a silver mirror was formed, and was filtered through Celite and concentrated under reduced pressure. Yield: 76 mg (quant.). ESI-MS m/z: 601.3 $[M\text{-}SbF_6]^+$ and 235.8 $[SbF_6]^-$. ^{1}H NMR ($CDCl_3$): 11.92 (br, s, 2H), 11.44 (br, s, 2H), 8.17 (br, s, 2H), 7.42 (br, s, 2H), 5.81 (br, s, 2H), 4.64 (m, 1H), 4.62 (m, 1H), 3.93 (br, m, 2H), 2.92 (m, 2H), 2.87 (m, 2H), 2.68 (s, 18H), 1.36 (s, 18H). Elem. Anal.: $C_{36}H_{54}CoF_6N_4Sb$ (837.52); Calcd. C, 51.63; H, 6.50; Co, 7.04; F, 13.61; N, 6.69; Sb, 14.54. Found: C, 51.06; H, 6.51; Co, 6.91; F, 13.77; N, 6.65; Sb, 15.07. Diffusion of pentane into a concentrated CH_2Cl_2 solution of **$(2)^{+}$•SbF_6^{-}** affords dark brown single crystals suitable for X-Ray diffraction studies.

Crystal structure analysis. A single crystal of **$(2)^{+}$•SbF_6^{-}** was dipped into a mixture of polyparafins then took up with a cryoloop and mounted on a Kappa CCD Nonius diffractometer equipped with graphite-monochromated Mo-Kα (λ = 0.71073 Å) and a cryostream cooler. Data collections were performed at 200 K. The cells were refined using the whole data respectively. Collected reflections were corrected for absorption,[16] Lorentz and polarization effects. The structures were solved by charge flipping method implemented by OLEX2 software[17] and refined using the parallelised version of SHELX 97[18] run under OLEX2. All non- hydrogen atoms were refined with anisotropic thermal parameters. Hydrogen atoms were generated in idealized positions, attached to the carrier atoms, with isotropic thermal parameters. Crystallographic data (excluding structure factors) for the structure reported in this paper have been deposited with the Cambridge Crystallographic Data Centre as supplementary publication no. CCDC-978151. Copies of the data can be obtained free of charge on application to CCDC, 12 Union Road, Cambridge CB21EZ, UK (fax: (+44)1223-336-033) or via http://www.ccdc.cam.ac.uk/conts/retrieving.html.

a)

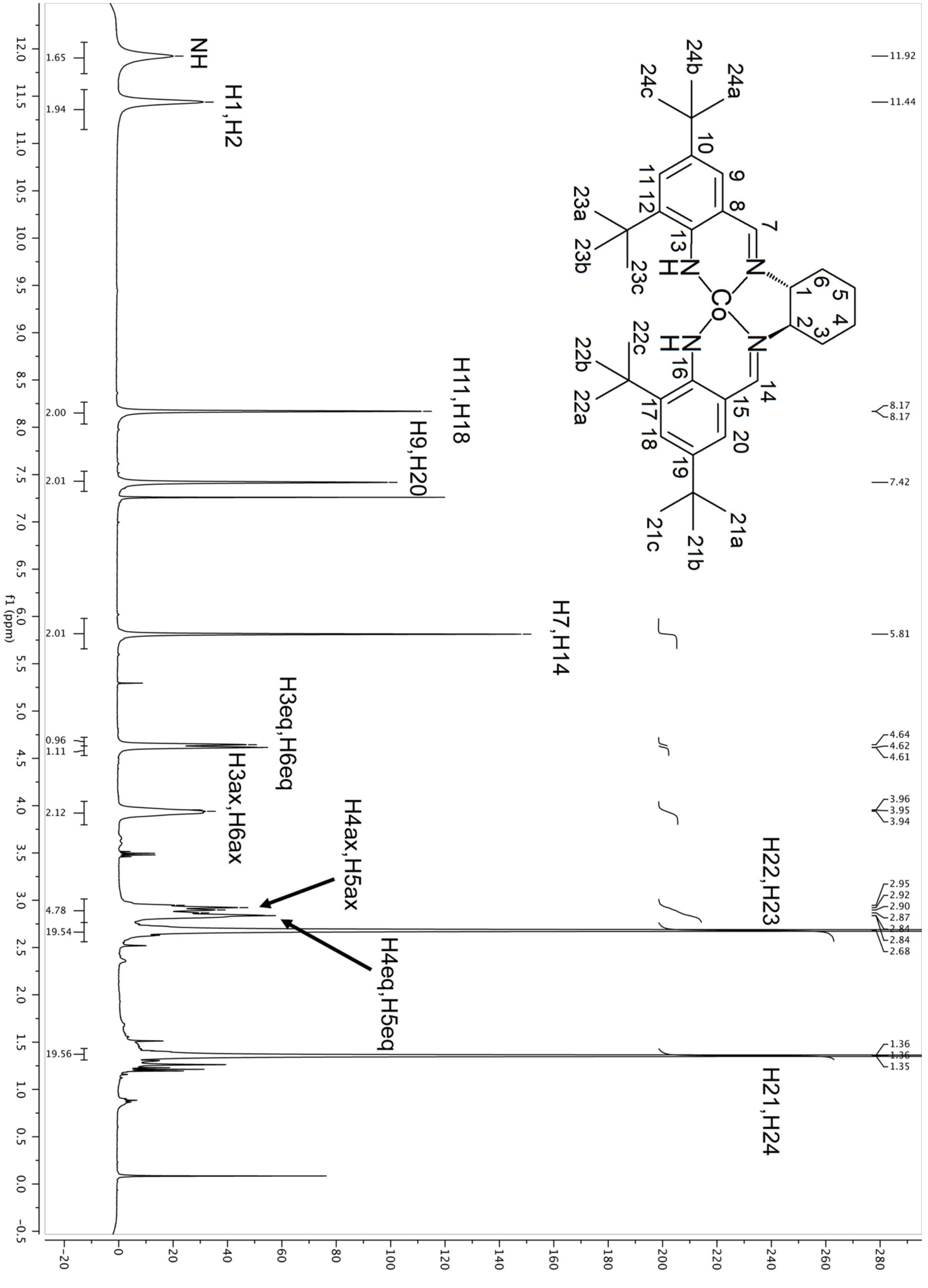

NH
H1,H2
H11,H18
H9,H20
H7,H14
H3eq,H6eq
H3ax,H6ax
H4ax,H5ax
H4eq,H5eq
H22,H23
H21,H24
Co
N
H
1.65
1.94
2.00
2.01
2.01
0.96
1.11
2.12
4.78
19.54
19.56
11.92
11.44
8.17
8.17
7.42
5.81
4.64
4.62
4.61
3.96
3.95
3.94
2.95
2.92
2.90
2.87
2.84
2.84
2.68
1.36
1.36
1.35
f1 (ppm)

b)

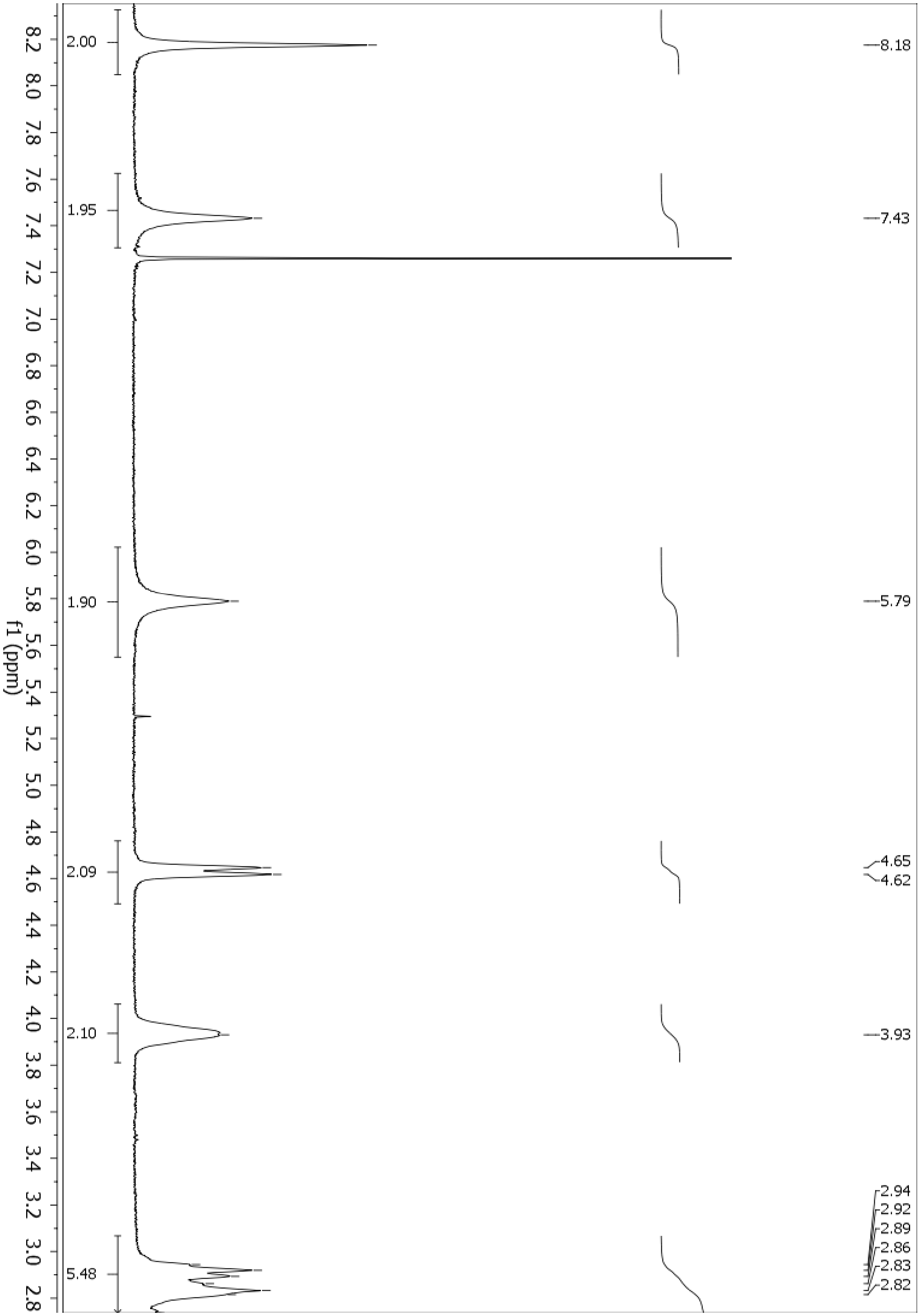

Figure S1. a) 1H NMR spectrum of **(2)$^+$.(SbF$_6$)$^-$** in CDCl$_3$ with assignments and b) zoom.

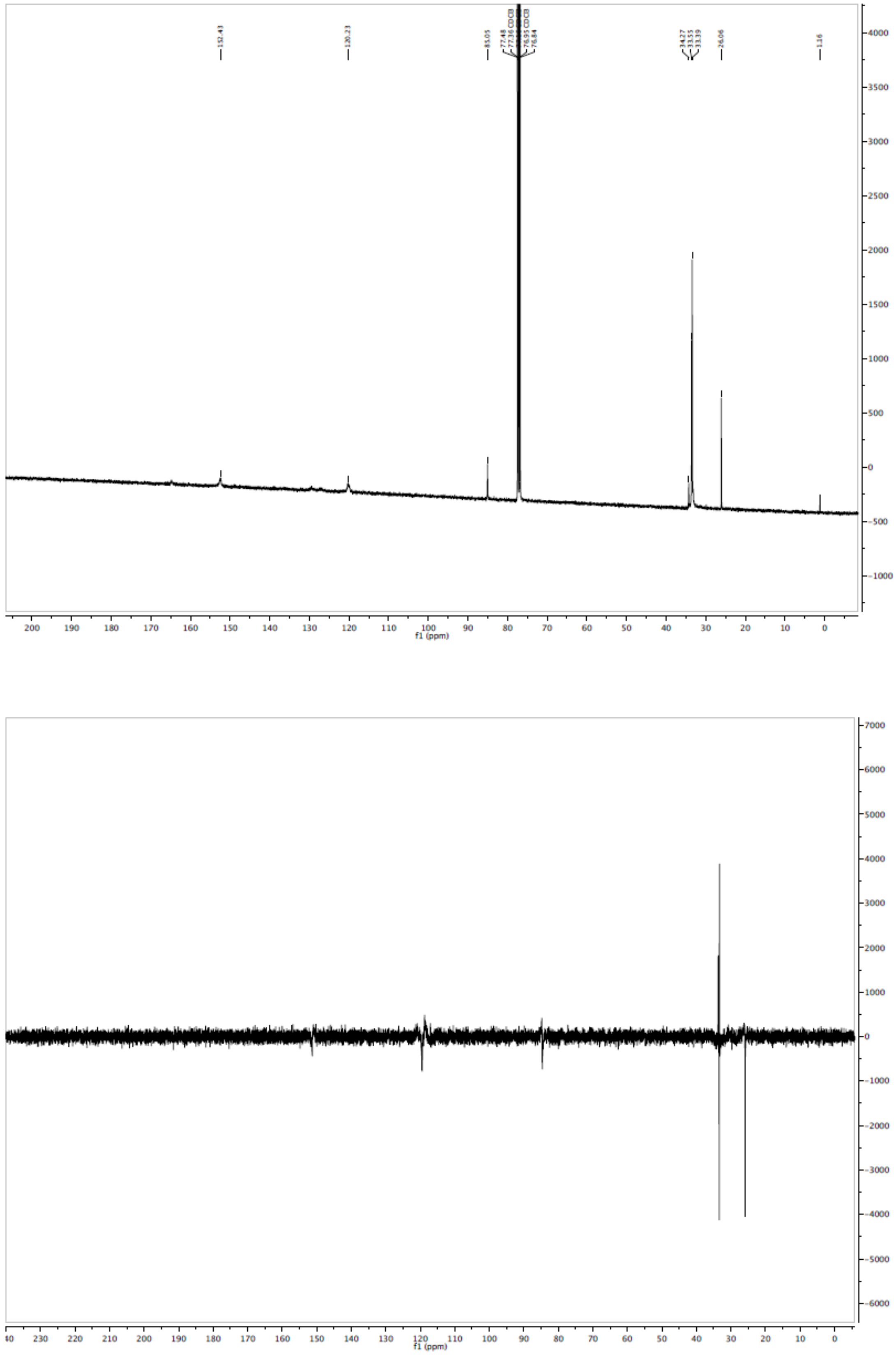

Figure S2. ^{13}C (top) and DEPT135 (bottom) NMR spectra of **(2)$^+$ • SbF$_6^-$** in CDCl$_3$

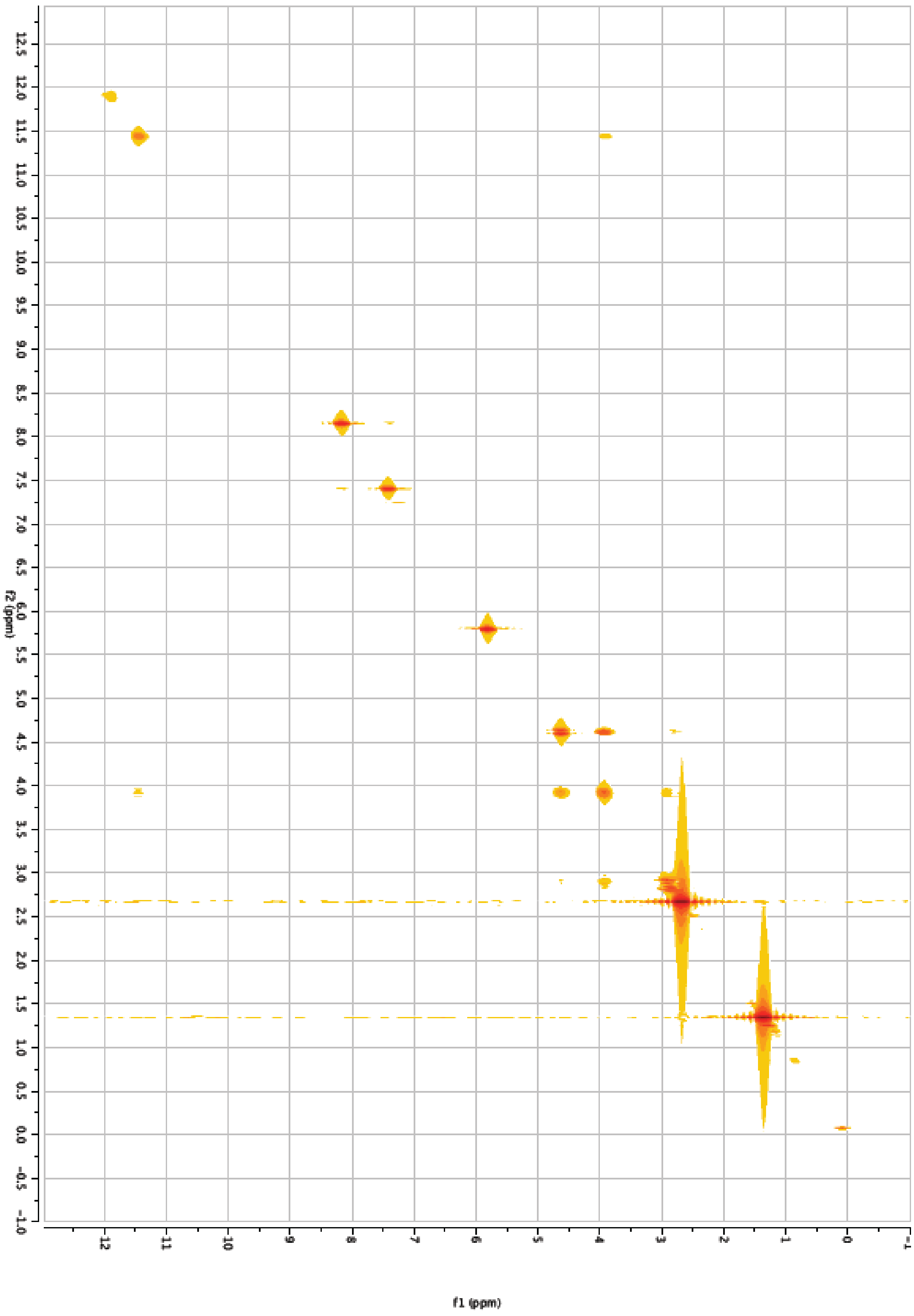

Figure S3. 2D COSY NMR spectrum of **(2)**$^+$ • **SbF$_6$**$^-$ in CDCl$_3$

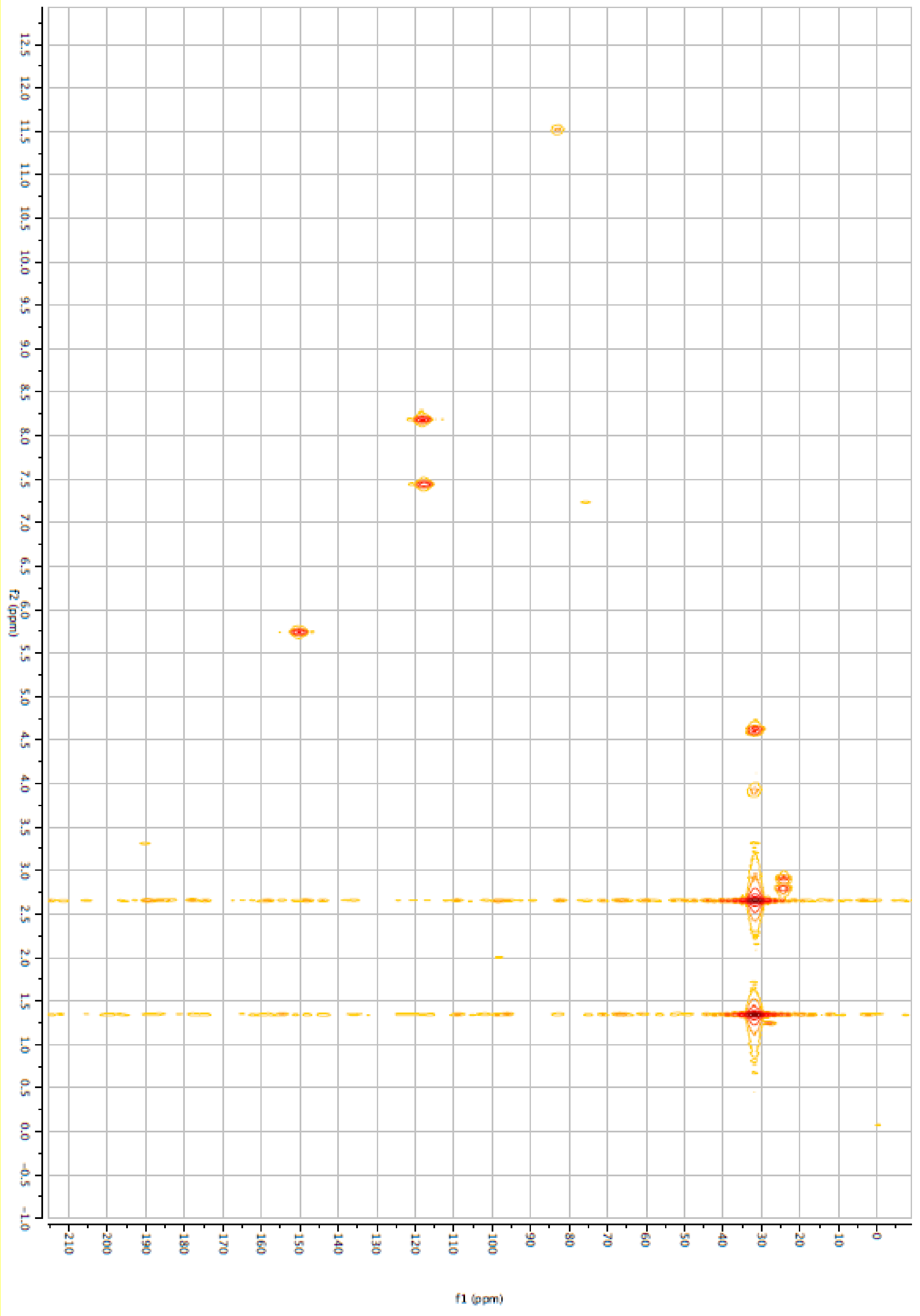

Figure S4. 2D HSQC NMR spectrum of **(2)$^+$ • SbF$_6^-$** in CDCl$_3$

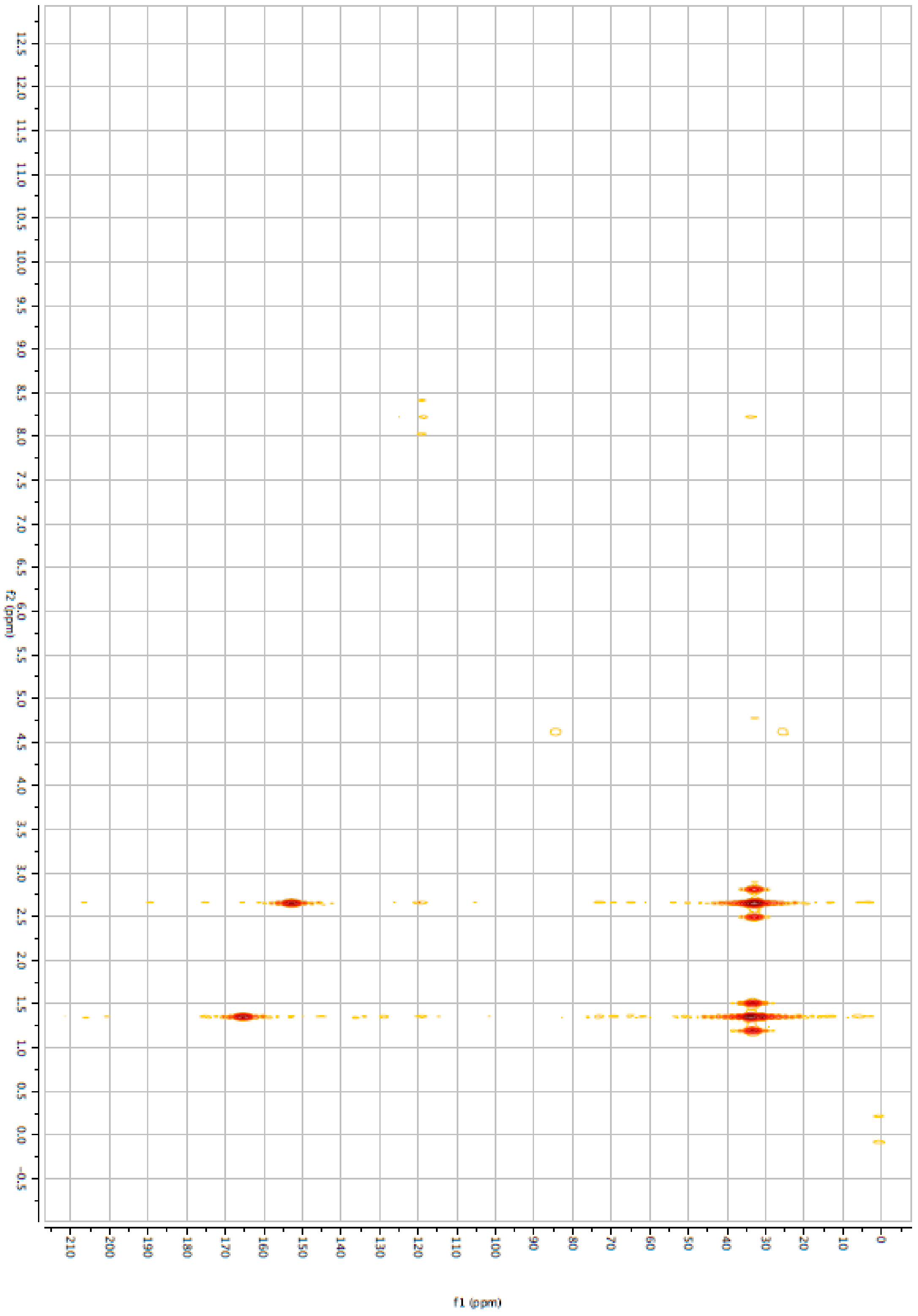

Figure S5. 2D HMBC NMR spectrum of **$(2)^+$ • SbF_6^-** in $CDCl_3$

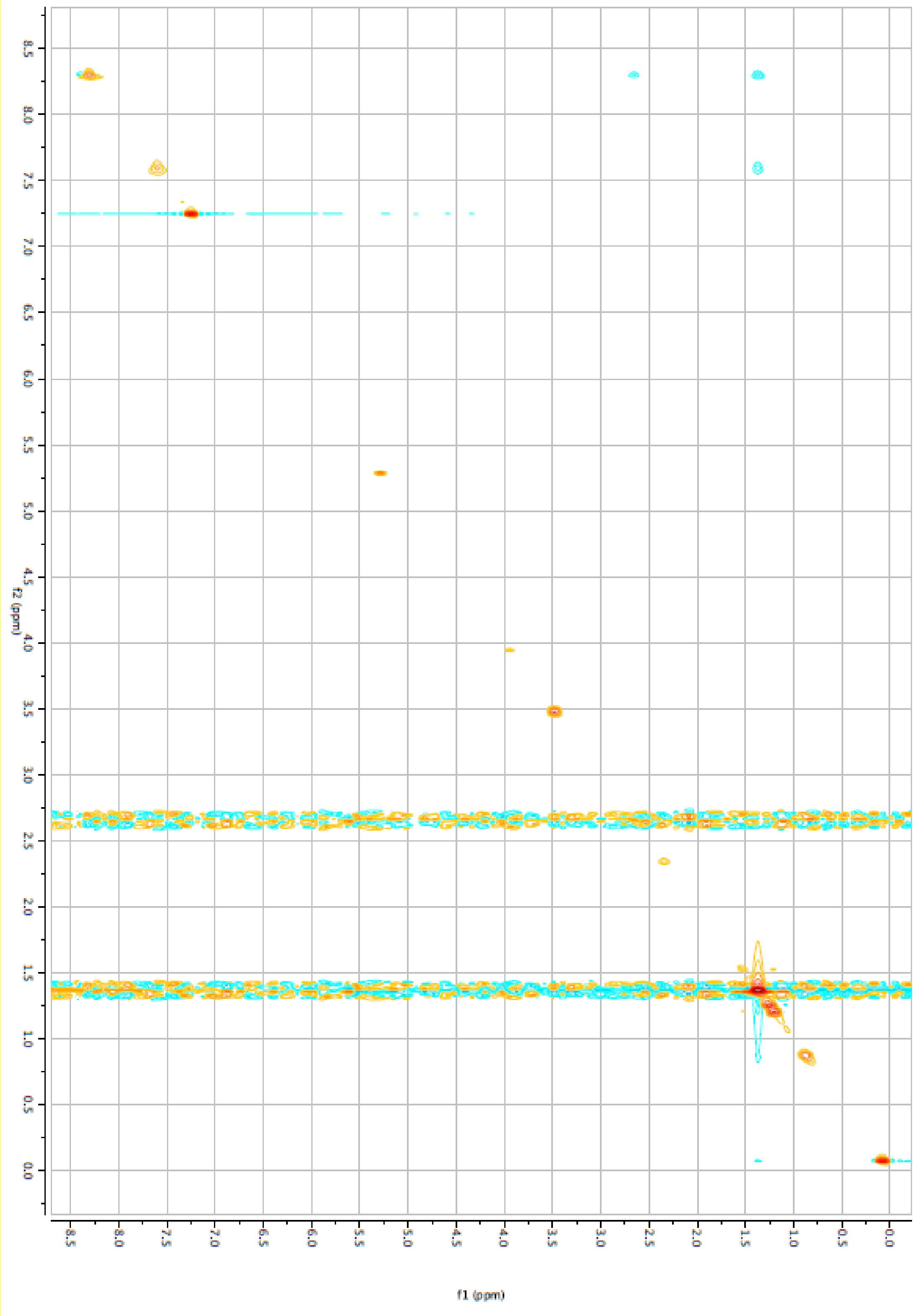

Figure S6. 2D NOESY NMR spectrum of **(2)$^+$ • SbF$_6^-$** in CDCl$_3$

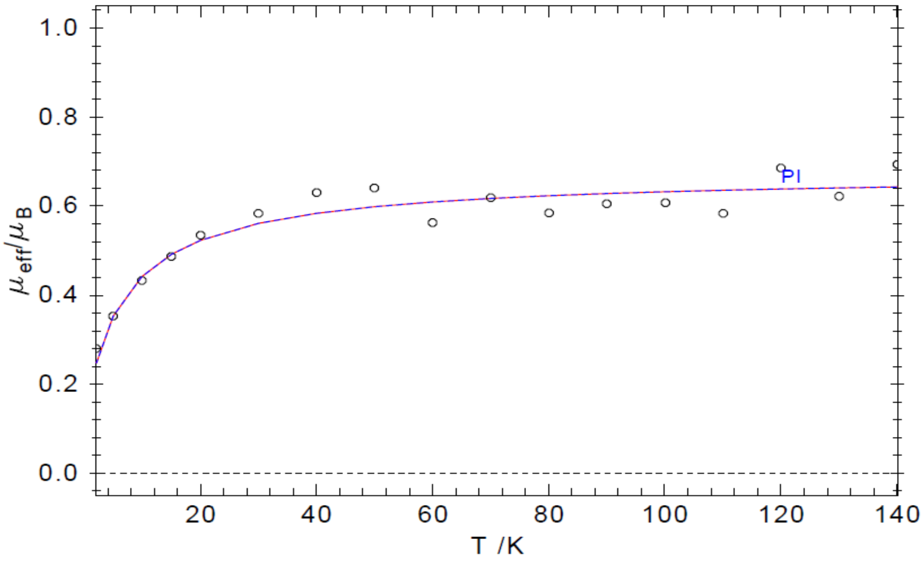

Figure S7. Temperature dependence of the magnetic moment of **(2)$^+$ • SbF$_6^-$** in CH_2Cl_2 solution; PI is from a 15% paramagnetic impurity (assuming S_{PI}=1/2), and the red line represents a simulation using the following parameters: $g_1 = g_2 = 2.00$, J = -574 cm^{-1} and χ_{TIP} = 2.15 10^{-3} e.m.u..

Table S1. Experimental and calculated first coordination sphere bond lengths (Å) for **2**, **(2)$^+$** and **(2)$^+$ • SbF$_6^-$** using BP86.[a]

Bond	**2** (exp)	**(2)$^+$ • SbF$_6^-$** (exp)	**2** (calc)	**(2)$^+$** (calc)	**(2)$^+$ • SbF$_6^-$** (calc)	**(2)$^+$** (calc)	**(2)$^+$ • SbF$_6^-$** (calc)
Nature		A B	doublet	triplet	triplet	singlet	singlet
Co-N1	1.855(3)	1.862(5)/1.867(6)	1.860	1.895	1.891	1.854	1.854
Co-N2	1.861(3)	1.850(5)/1.863(5)	1.861	1.896	1.894	1.853	1.852
Co-N3	1.842(3)	1.828(5)/1.832(5)	1.853	1.835	1.843	1.826	1.827
Co-N4	1.844(3)	1.815(6)/1.810(5)	1.852	1.836	1.838	1.824	1.827
C-N3	1.336(5)	1.346(8)/1.346(8)	1.352	1.361	1.362	1.352	1.355
C-N4	1.338(5)	1.350(8)/1.356(8)	1.353	1.362	1.363	1.353	1.351

[a]: Atom numbering used:

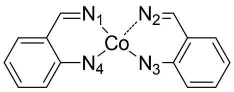

Table S2. Calculated first coordination sphere bond lengths (Å) for **(2)**$^+$ in the triplet and singlet states (S = 0) from BS(1,1) B3LYP calculations.[a]

Bond	**(2)**$^+$ (calc)	**(2)**$^+$ (calc)
Nature	triplet	singlet
Co-N1	1.913	1.902
Co-N2	1.909	1.899
Co-N3	1.840	1.882
Co-N4	1.837	1.879
C-N3	1.358	1.341
C-N4	1.358	1.342

[a]: Atom numbering used:

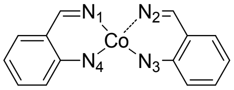

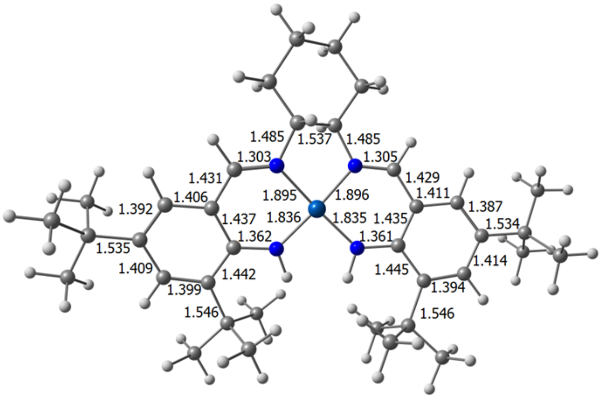

Figure S8. Geometry optimized structure of **(2)**$^+$ without counter ion and selected bond distances in the triplet state (using BP86).

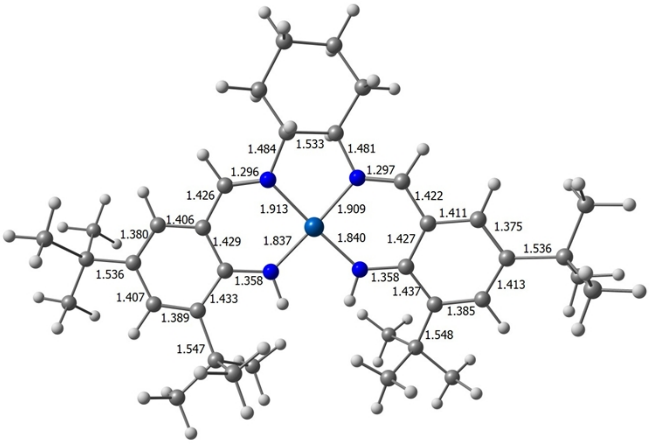

Figure S9. Geometry optimized structure of **(2)**$^+$ without counter ion and selected bond distances in the triplet state (using B3LYP).

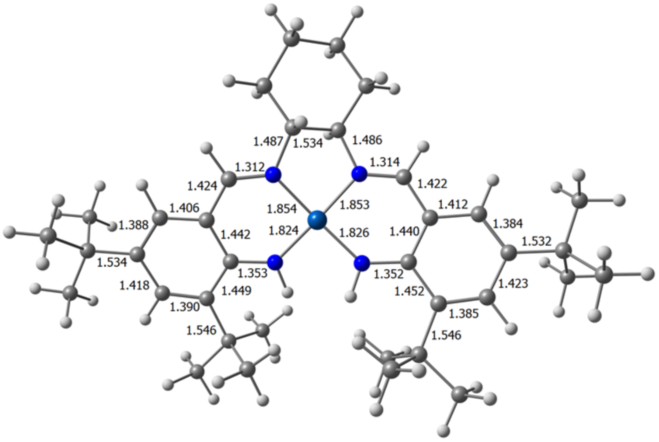

Figure S10. Geometry optimized structure of **(2)**$^+$ and selected bond distances in the singlet state (using BP86).

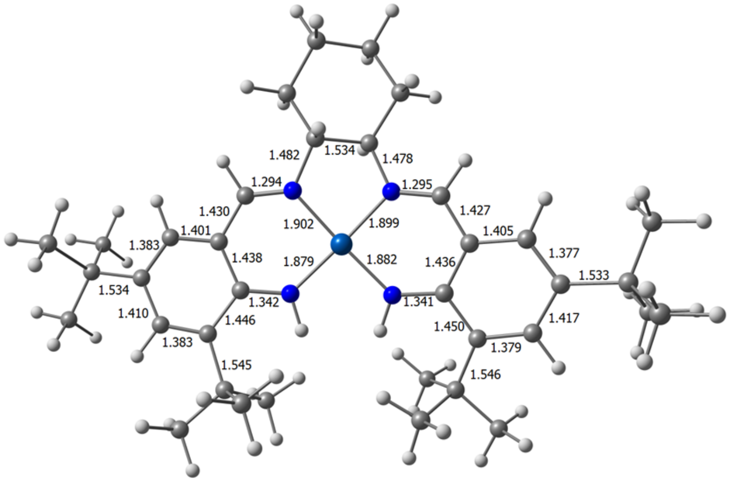

Figure S11. Geometry optimized structure of **(2)**$^+$ without counter ion and selected bond distances in the singlet state obtained from a BS(1,1) B3LYP calculation.

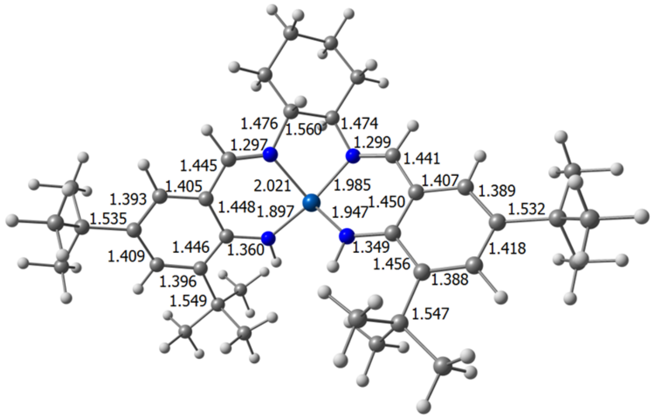

Figure S12. Geometry optimized structure of **(2)**$^+$ and selected bond distances in the quintet state (using BP86). The triplet state is found to be favored in energy by 25 kcal.mol^{-1} over the quintet state.

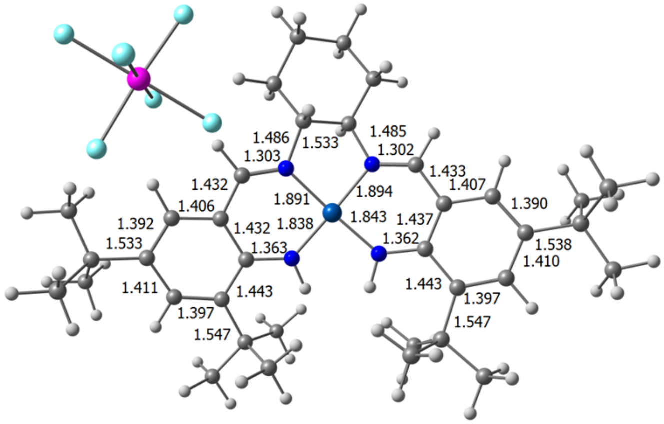

Figure S13. Geometry optimized structure of **(2)$^+$.SbF$_6^-$** and selected bond distances in the triplet state (using BP86).

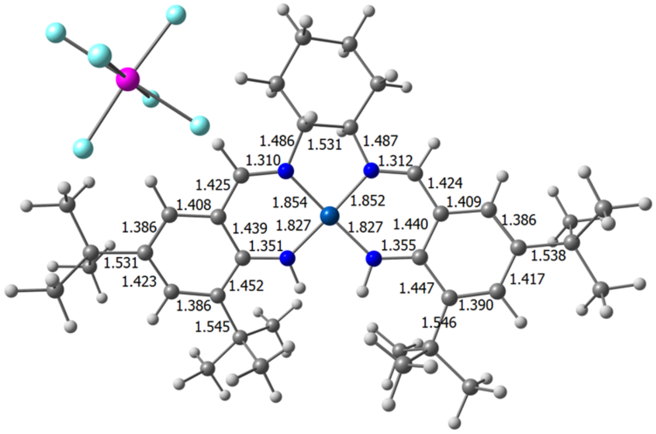

Figure S14. Geometry optimized structure of **(2)$^+$.SbF$_6^-$** and selected bond distances in the singlet state (using BP86).

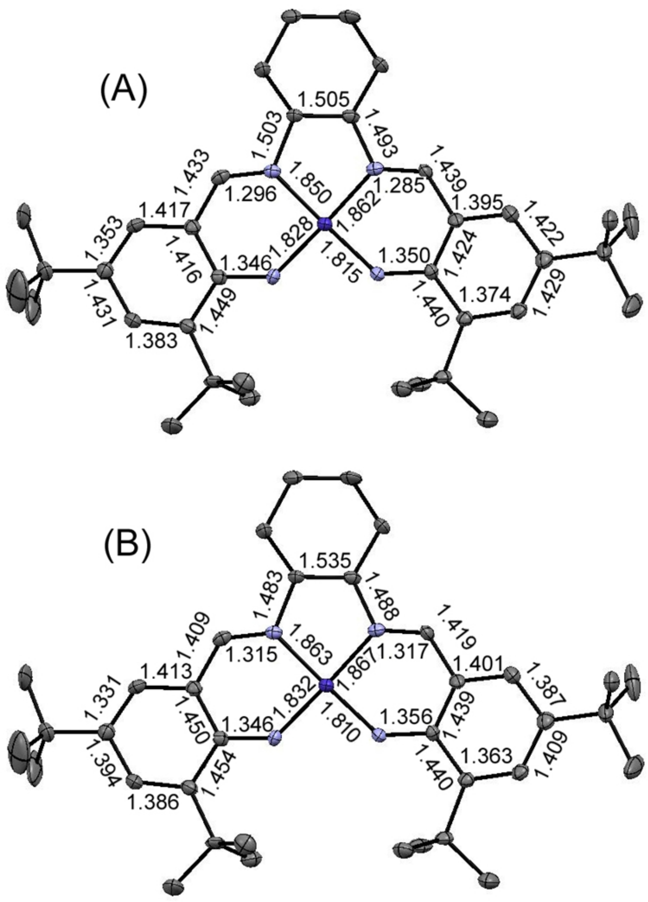

Figure S15. Selected bond distances in the two distinct molecules (A and B) present in the crystal cell of **(2)$^+$.SbF$_6^-$**.

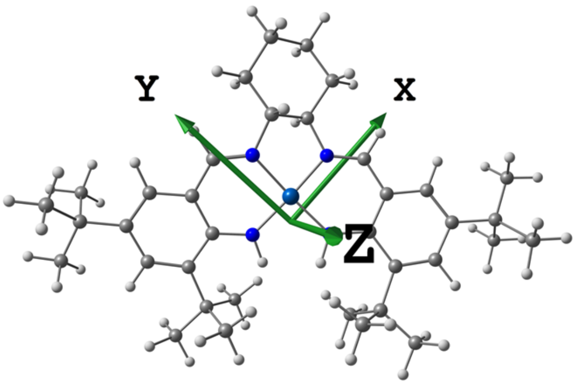

Figure S16. Axes system used.

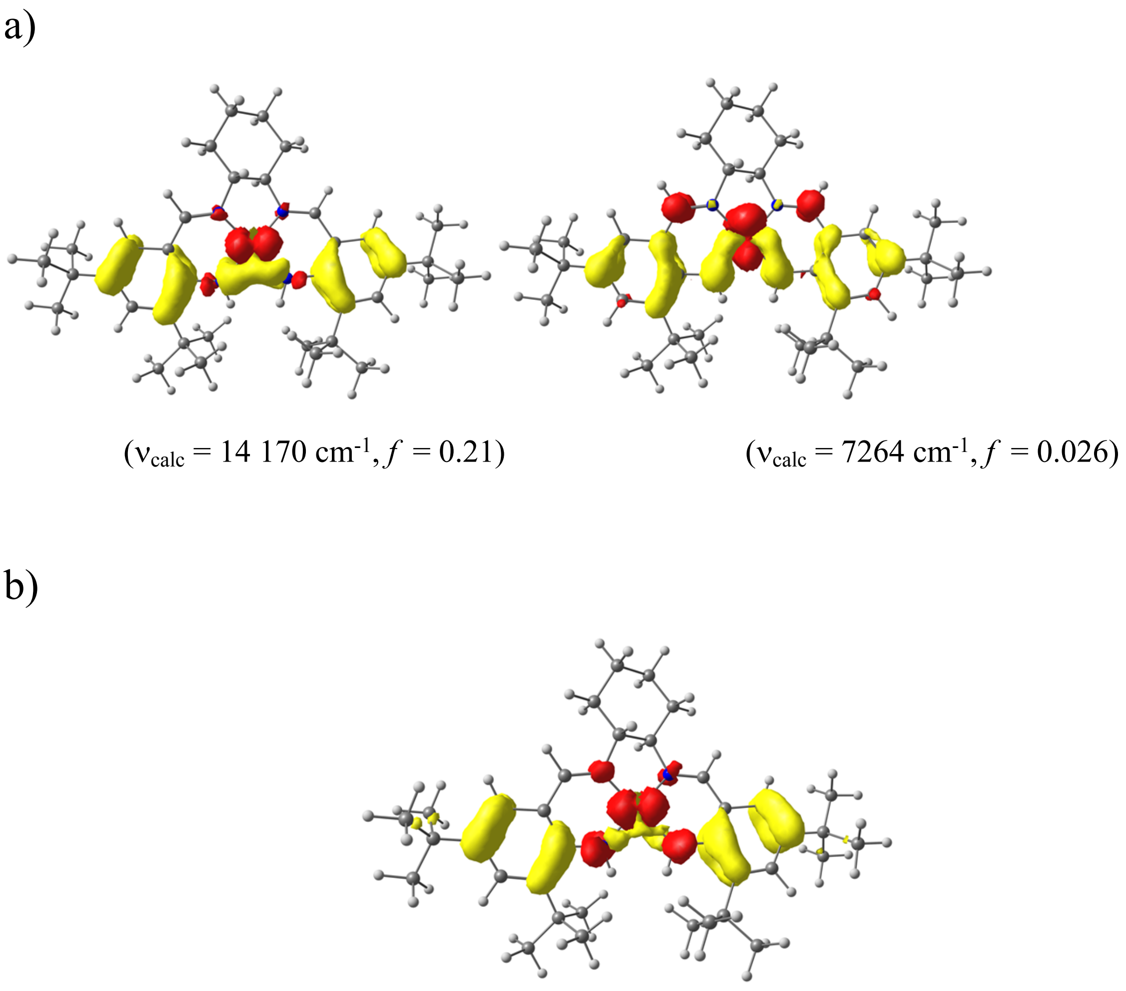

(ν_{calc} = 14 170 cm^{-1}, f = 0.21) (ν_{calc} = 7264 cm^{-1}, f = 0.026)

(ν_{calc} = 17047 cm^{-1}, f = 0.77)

Figure S17. TD-DFT assignment of the electronic transitions of **(2)**$^+$ by considering: a) a triplet spin state and b) a closed-shell singlet spin state. The diagrams give the difference electron densities, where red corresponds to positive density and yellow to negative density.

References

[1] F. Neese, F. *WIREs Comput. Mol. Sci.* 2012, **2**, 73.

[2] J. P. Perdew, *Phys. Rev. B,* 1986, **33**, 8822. (b) J. P. Perdew, *Phys. Rev. B,* 1986, **34**, 7406.

[3] A. D. Becke, *Phys. Rev. A,* 1988, **38**, 3098.

[4] F. Weigend, R. Ahlrichs, *Phys. Chem. Chem. Phys.,* 2005, **7**, 3297.

[5] F. Neese, *J. Comp. Chem.,* 2003, **24**, 1740.

[6] A. Weigend, *Phys. Chem. Chem. Phys.,* 2006, **8**, 1057.

[7] A. Klamt, G. Schürmann, G. *J. Chem. Soc., Perkin Trans. 2,* 1993, 793.

[8] A. D. Becke, *J. Chem. Phys.,* 1993, **98**, 5648.

[9] C. Lee, W. Yang, R. G. Parr, *Phys. Rev., B,* 1988, **37**, 785.

[10] M. E. Casida, in *Recent Advances in Density Functional Methods*, ed. D. P. Chong, World Scientific, Singapore, 1995.

[11] R. E. Stratmann, G. E. Scuseria, M. J. Frisch, *J. Chem. Phys.,* 1998, **109**, 8218.

[12] R. Bauernschmitt, R. Ahlrichs, *Chem. Phys. Lett.,* 1996, 454.

[13] S. Hirata, M. Head-Gordon, *Chem. Phys. Lett.,* 1999, **314**, 291.

[14] S. Hirata, M. Head-Gordon, *Chem. Phys. Lett.,* 1999, **302**, 375.

[15] F. Neese, G. Olbrich, *Chem. Phys. Lett.,* 2002, **362**, 170.

[16] SADABS, Bruker–Siemens Area Detector Absorption and Other Correction, G. M. Sheldrick, University of Göttingen, Germany, 2006, Version 2008/1.

[17] O. V. Dolomanov, L. J. Bourhis, R. J. Gildea, J. A. K. Howard, H. Puschmann, *J. Appl. Cryst.* 2009, **42**, 339.

[18] G. M. Sheldrick, *Acta Crystallogr.*, 2008, **A64**, 112.